Anisotropic Optical Shock Waves in Isotropic Media with Giant Nonlocal Nonlinearity

Giulia Marcucci,[1,2,*,‡] Xubo Hu,[3,4] Phillip Cala,[3] Weining Man,[3] Davide Pierangeli,[1,2] Claudio Conti,[2,1,5] and Zhigang Chen[3,5,†]

[1]*Department of Physics, Sapienza University, P.le Aldo Moro 2, 00185 Rome, Italy*
[2]*Institute for Complex Systems, Via dei Taurini 19, 00185 Rome, Italy*
[3]*Department of Physics and Astronomy, San Francisco State University, San Francisco, California 94132, USA*
[4]*College of Electronics Engineering, South China Agricultural University, Guangzhou 510642, China*
[5]*TEDA Applied Physics Institute and School of Physics, Nankai University, Tianjin 300457, China*

(Received 10 September 2019; revised 5 September 2020; accepted 27 October 2020; published 10 December 2020)

Dispersive shock waves in thermal optical media are nonlinear phenomena whose intrinsic irreversibility is described by time asymmetric quantum mechanics. Recent studies demonstrated that the nonlocal wave breaking evolves in an exponentially decaying dynamics ruled by the reversed harmonic oscillator, namely, the simplest irreversible quantum system in the rigged Hilbert spaces. The generalization of this theory to more complex scenarios is still an open question. In this work, we use a thermal third-order medium with an unprecedented giant Kerr coefficient, the m-cresol/nylon mixed solution, to access an extremely nonlinear, highly nonlocal regime and realize anisotropic shock waves with internal gaps. We compare our experimental observations to results obtained under similar conditions but in hemoglobin solutions from human red blood cells, and found that the gap formation strongly depends on the nonlinearity strength. We prove that a superposition of Gamow vectors in an *ad hoc* rigged Hilbert space, that is, a tensorial product between the reversed and the standard harmonic oscillators spaces, describes the beam propagation beyond the shock point. The anisotropy turns out from the interaction of trapping and antitrapping potentials. Our work furnishes the description of novel intriguing shock phenomena mediated by extreme nonlinearities.

DOI: 10.1103/PhysRevLett.125.243902

Dispersive shock waves (DSWs) are widespread phenomena in physics—from hydrodynamics [1–3] to acoustics [4], from Bose–Einstein condensates [5–10] to plasmas [11], and from quantum liquids [12] to optics [13–35].

In photonics, when light propagates in a medium whose refractive index depends on the beam intensity, (e.g., through the Kerr effect [36]), the interplay between diffraction (or dispersion) and nonlinearity can lead to steep gradients in the phase profile and, in some cases, to a wave breaking [35]. Such discontinuity is regularized by rapid oscillations in phase chirp and in intensity outlines called undular bores [18]. If we mutate this third-order nonlinearity, making it nonlocal (or noninstantaneous), then the dynamics may have some changes. When the phase chirp reaches the discontinuity and starts oscillating, the intensity does not develop undular bores but rather the annular collapse singularity [27,28,35,37]. Spatial collapse of DSWs occurs in thermal media, where the thermo-optic effect leads the light-matter interaction and the refractive index perturbation depends on the whole intensity profile [35,36].

Theoretically, such modification of the Kerr nonlinearity has significant consequences. Laser beam propagation in a standard Kerr medium is ruled by the nonlinear Schrödinger equation (NLSE), which is exactly solvable by the inverse scattering transform method [38–40]. However, the NLSE with a nonlocal potential cannot be solved by inverse scattering transform [despite some recent progress in two-dimensional (2D) media [41,42]] but only through the Whitham modulation and the hydrodynamic approximation [43]. Moreover, the dynamics beyond the shock appears to be intrinsically irreversible, as recently shown by applying time asymmetric quantum mechanics [44–55] to the description of DSWs in highly nonlocal approximation [25,26,28,35,56].

Light propagation beyond the collapse is then expressed as a superposition of unbounded eigenfunctions called Gamow vectors (GVs) [55,57,58], which exponentially decay with quantized decay rates. Such light wave evolution is the outcome of a phenomenon, the shock, that is intrinsically irreversible. In this case, *irreversibility* means that there is no way to get the initial Gaussian beam back from the final output after the wave breaking: even in the absence of appreciable absorption and interaction with an external thermal bath, the dynamics cannot be inverted, i.e., it is time asymmetric. Can this theoretical model be used to describe much more complex scenarios? To answer this question, we need to access regimes with much stronger nonlinearity.

In recent experiments, it is shown that m-cresol/nylon solutions exhibit an isotropic giant self-defocusing nonlinearity [59]. M-cresol/nylon is a thermal chemical mixture consisting of an organic solvent (m-cresol) and a

synthetic polymeric solute (nylon). When it is illuminated by a cw laser beam, light absorption induces heat, which reduces the refractive index: the material experiences a large thermo-optical effect made nonlocal by the heat diffusion. Since the temperature changes with the beam intensity, this nonlinearity follows a nonlocal Kerr model. The Kerr coefficient n_2 of pure m-cresol is -9×10^{-8} cm^2/W, but in mixtures with nylon the coefficient can be as high as $n_2=-1.6\times10^{-5}$ cm^2/W for a nylon mass concentration of 3.5%, orders of magnitude higher than other thermal nonlinear materials in which annual collapse singularities have been observed [35].

In this Letter, we report on our theoretical discovery and experimental evidence of optical DSWs with an *anisotropic zero singularity* (ZS) (i.e., a gap in the intensity profile along only one direction) in m-cresol/nylon solutions. The shock does develop an annular collapse, but around the ZS it presents an abrupt intensity discontinuity. We theoretically analyze this anisotropic wave breaking. Although the phenomenon of shock-wave interaction observed here is classical, the underlying physics is explained exactly by the theory based on time asymmetric quantum mechanics. In our approach, the nonlocal nonlinear potential that rules the light-matter interaction acts like a specific linear operator, whose shape depends on the initial condition. By a convolution reduction [60], we transform a classical NLSE into a linear Schrödinger equation acting on a rigged Hilbert space [46]. We model the beam propagation beyond the shock point and uncover the mechanism that determines how such an abrupt intensity discontinuity is generated. We numerically simulate these results and find remarkable agreement between experimental observations and theoretical predictions. Experiments were carried out also in hemoglobin solutions with similar thermal nonlinearity, and we found that the gap formation strongly depends on the nonlinearity strength. The results we found are general, and our theory can be applied to other physical systems with high nonlinearity, e.g., plasmonic nanosuspensions [61], Bose–Einstein condensates [9,62], or saturable defocusing atomic vapors, where the evolution leads to dark soliton instability [63].

For a laser beam propagating in a thermal medium with refractive index $n=n_0+\Delta n[|A|^2](\mathbf{R})$, where $\mathbf{R}=(\mathbf{R}_\perp,Z)=(X,Y,Z)$, the NLSE describes the evolution of the envelope $A(\mathbf{R})$ of the monochromatic field $\mathbf{E}(\mathbf{R})=\hat{\mathbf{E}}_0A(\mathbf{R})e^{ikZ}$. It reads as

$$2ik\partial_ZA+\nabla^2_{\mathbf{R}_\perp}A+2k^2\frac{\Delta n[|A|^2]}{n_0}A=-i\frac{k}{L_{\rm loss}}A,$$

where $\nabla^2_{\mathbf{R}_\perp}=\partial^2_X+\partial^2_Y$, $k=(2\pi n_0/\lambda)$ is the wave number, λ is the wavelength, and $L_{\rm loss}$ is the linear loss length. By defining the intensity $I=|A|^2$, the power $\bar{P}(Z)=\iint d\mathbf{R}_\perp I(\mathbf{R})$, the diffraction length $L_d=kW_0^2$ with W_0 the initial beam waist, and $\alpha=L_d/L_{\rm loss}$, one can see that $\bar{P}$ is not conserved only if $\alpha\neq0$. Indeed, if $\alpha\sim0$, then $\partial_ZI(\mathbf{R})\sim0$ [64] and $\Delta n[|A|^2]=\Delta n[|A|^2](\mathbf{R}_\perp)$, as obtained from the derivation of the refractive index perturbation from the heat equation in parabolic approximation [35].

It turns out that, in low absorption regime, the refractive index perturbation in our NLSE is [35] $\Delta n[|A|^2](\mathbf{R}_\perp)=n_2\iint d\mathbf{R}'_\perp\mathcal{K}(\mathbf{R}_\perp-\mathbf{R}'_\perp)I(\mathbf{R}'_\perp)$, with n_2 the Kerr coefficient and $\mathcal{K}(\mathbf{R}_\perp)$ the kernel function describing the nonlocal nonlinearity, normalized such that $\iint d\mathbf{R}_\perp\mathcal{K}(\mathbf{R}_\perp)=1$. For $\mathcal{K}(\mathbf{R}_\perp)=\delta(\mathbf{R}_\perp)$ we attain the well-known local Kerr effect, i.e., $n=n_0+n_2I$ [36]. In our nonlocal case, where the laser beam produces a thermo-optic effect that generates an isotropic variation of the medium density distribution, the response function is $\mathcal{K}(X,Y)=(1/2\pi L^2_{\rm nloc})K_0(\sqrt{X^2+Y^2}/L_{\rm nloc})$, with K_0 the modified Bessel function and $L_{\rm nloc}$ the nonlocality length [17,34,65–67]. We rescale our NLSE with $\alpha\sim0$ by defining the dimensionless variables $x=X/W_0$, $y=Y/W_0$, and $z=Z/L_d$. We obtain

$$i\partial_z\psi+\frac{1}{2}\nabla^2_{\mathbf{r}_\perp}\psi+\chi PK*|\psi|^2\psi=0, \tag{1}$$

where $\mathbf{r}=(\mathbf{r}_\perp,z)=(x,y,z)$, $\nabla^2_{\mathbf{r}_\perp}=\partial^2_x+\partial^2_y$, $\psi(\mathbf{r})=(W_0/\sqrt{\bar{P}})A(\mathbf{R})$, $\chi=n_2/|n_2|$ and $P=\bar{P}/P_{\rm REF}$ with $P_{\rm REF}=\lambda^2/4\pi^2n_0|n_2|$. The asterisk in Eq. (1) stands for the convolution product, while $K(x,y)=W_0^2\mathcal{K}(X,Y)=(1/2\pi\sigma^2)K_0(\sqrt{x^2+y^2}/\sigma)$, with $\sigma=L_{\rm nloc}/W_0$ the nonlocality degree.

In highly nonlocal approximation ($\sigma\gg1$), even if the parabolic approximation for the NLSE does not always work [68], in our case $|\psi|^2$ mimics a delta function (or a narrow superposition of delta functions), and the nonlocal potential loses its I dependence, becoming a simple function of the transverse coordinates [65,69], that is, $K*|\psi|^2\simeq\Delta(\mathbf{r}_\perp)$, with

$$\begin{aligned}\Delta(\mathbf{r}_\perp)\simeq{}&\Delta(\mathbf{0})+(\partial_x\Delta|_{\mathbf{r}_\perp=\mathbf{0}})x+(\partial_y\Delta|_{\mathbf{r}_\perp=\mathbf{0}})y\\&+\frac{1}{2}(\partial^2_x\Delta|_{\mathbf{r}_\perp=\mathbf{0}})x^2+(\partial_x\partial_y\Delta|_{\mathbf{r}_\perp=\mathbf{0}})xy\\&+\frac{1}{2}(\partial^2_y\Delta|_{\mathbf{r}_\perp=\mathbf{0}})y^2\end{aligned} \tag{2}$$

after a Taylor second-order expansion. This approximation maps the NLSE in Eq. (1) into a linear Schrödinger equation $i\partial_z\psi(\mathbf{r})=\hat{H}(\mathbf{p}_\perp,\mathbf{r}_\perp)\psi(\mathbf{r})$, with $\hat{H}(\mathbf{p}_\perp,\mathbf{r}_\perp)=\frac{1}{2}\hat{\mathbf{p}_\perp}^2+\hat{V}(\mathbf{r}_\perp)$ the Hamiltonian, $\hat{\mathbf{p}}_\perp=(\hat{p}_x,\hat{p}_y)=(-i\partial_x,-i\partial_y)$ the transverse momentum, and $\hat{V}(\mathbf{r}_\perp)=-\chi P\Delta(\mathbf{r}_\perp)\mathbb{1}$ the multiplicative potential ($\mathbb{1}$ is the identity operator). Let us consider the initial condition

$$\psi_{\rm ISO}(\mathbf{r}_\perp)=\psi_{\rm even}(x)\psi_{\rm even}(y),\quad \psi_{\rm even}(x)=\frac{1}{\sqrt[4]{\pi}}e^{-x^2/2} \tag{3}$$

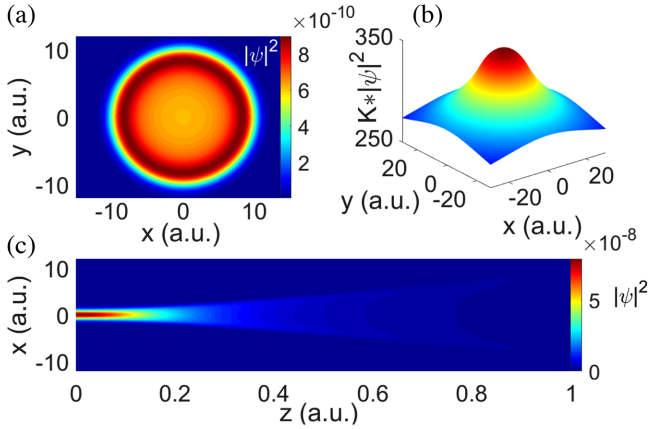

FIG. 1. Solution of the NLSE, Eq. (1), with a symmetric initial condition, Eq. (3), for $P = 4 \times 10^6$ and $\sigma = 120$ in arbitrary units: (a) shows the intensity transverse profile at $z = 1$; (b) exhibits the symmetric nonlinear potential; (c) reports the intensity longitudinal outline, showing the side view of propagation on the plane (x, z) equal to one on the plane (y, z).

The shape of $\Delta(\mathbf{r}_\perp)$ depends on $|\psi_{\rm ISO}(\mathbf{r}_\perp)|^2$. Indeed, since the square of an absolute value is an even function, all the first derivatives in Eq. (3) vanish—hence $\Delta(\mathbf{r}_\perp) \simeq \Delta_0^2 - \frac{1}{2}\Delta_2^2|\mathbf{r}_\perp|^2$ where $\Delta_0^2 = 1/4\sigma^2$ and $\Delta_2^2 = 1/2\sqrt{\pi}\sigma^3$. More details are reported in the Supplemental Material [70].

In the defocusing case ($n_2 < 0$), Fig. 1(a) shows the transverse profile of the solution of Eq. (1) with the initial condition Eq. (3). Figure 1(b) exhibits the central part of the symmetric nonlinear potential $K * |\psi|^2$ without approximations (but for a high value of σ), while Fig. 1(c) reports the longitudinal profile on x, z (equal to the profile on y, z), showing the side view of the beam propagation. The corresponding Hamiltonian reads $\hat{H} = P\Delta_0^2 + \hat{H}_{\rm RHO}(p_x, x) + \hat{H}_{\rm RHO}(p_y, y)$, where $\hat{H}_{\rm RHO}(p_x, x) = \frac{1}{2}\hat{p}_x^{\,2} - (\gamma^2/2)\hat{x}^2$ is the 1D reversed harmonic oscillator (RHO) Hamiltonian of frequency $\gamma = \sqrt{P}\Delta_2$. Once moved to $\phi(\mathbf{r}) = e^{iP\Delta_0^2}\psi(\mathbf{r})$, the Schrödinger equation becomes $i\partial_z\phi(\mathbf{r}) = [\hat{H}_{\rm RHO}(p_x, x) + \hat{H}_{\rm RHO}(p_y, y)]\phi(\mathbf{r})$, which is completely separable. In bra-ket notation

$$
\begin{aligned}
i\frac{\mathrm{d}}{\mathrm{d}z}|\phi(z)\rangle &= \hat{H}_{\rm ISO}(\mathbf{p}_\perp, \mathbf{r}_\perp)|\phi(z)\rangle, \\
\hat{H}_{\rm ISO}(\mathbf{p}_\perp, \mathbf{r}_\perp) &= \hat{H}_{\rm RHO}(p_x, x) \otimes \mathbb{1}_y + \mathbb{1}_x \otimes \hat{H}_{\rm RHO}(p_y, y), \\
|\phi(z)\rangle &= |\phi_{\rm even}(z)\rangle_x \otimes |\phi_{\rm even}(z)\rangle_y, \qquad (4)
\end{aligned}
$$

with $\otimes$ the tensorial product, no more explicitly written hereafter. The solution of Eq. (4) lives in a tensorial product between two 1D rigged Hilbert spaces. Indeed, if we consider the evolution operator $\hat{U}(z) = e^{-i\hat{H}z}$ such that $|\phi(z)\rangle = \hat{U}(z)|\phi(0)\rangle$, for Eq. (4) we obtain $|\phi(z)\rangle = e^{-i\hat{H}_{\rm RHO}z}|\psi_{\rm even}\rangle_x e^{-i\hat{H}_{\rm RHO}z}|\psi_{\rm even}\rangle_y$. The representation of $|\phi_{\rm even}(z)\rangle_{x,y} = e^{-i\hat{H}_{\rm RHO}z}|\psi_{\rm even}\rangle_{x,y}$ in terms of GVs was already studied and was also already demonstrated to describe 1D DSWs in thermal media [25,26,28,35,56]. It is $|\phi_{\rm even}(z)\rangle_{x,y} = |\phi_N^G(z)\rangle + |\phi_N^{BG}(z)\rangle$, with $|\phi_N^G(z)\rangle = \sum_{n=0}^N e^{-\gamma/2(2n+1)z}|\mathfrak{f}_n^-\rangle\langle\mathfrak{f}_n^+|\psi_{\rm even}\rangle$ the decaying superposition of Gamow states $|\mathfrak{f}_n^-\rangle$, corresponding to the energy levels $E_n^{\rm RHO} = i(\gamma/2)(2n+1)$, and $|\phi_N^{\rm BG}(z)\rangle$ the background function, both belonging to the same rigged Hilbert space (see the Supplemental Material [70] for more details).

We consider also the following asymmetric initial condition:

$$
\psi_{\rm ANI}(\mathbf{r}_\perp) = \psi_{\rm odd}(x)\psi_{\rm even}(y), \qquad \psi_{\rm odd}(x) = -\frac{\sqrt{2}}{\sqrt[4]{\pi}}xe^{-x^2/2}, \qquad (5)
$$

$\psi_{\rm even}(y) = (1/\sqrt[4]{\pi})e^{-y^2/2}$ as in Eq. (3). In this case, Eq. (2) is reduced to $\Delta(\mathbf{r}_\perp) \simeq \Delta_0^2 + \frac{1}{2}\Delta_1^2x^2 - \frac{1}{2}\Delta_2^2y^2$, with $\Delta_0^2 = 1/4\sigma^2$, $\Delta_1^2 = 1/4\sigma^4$, and $\Delta_2^2 = 1/(2\sqrt{\pi}\sigma^3)$.

The consequent anisotropy appears evident: not only the initial condition presents a ZS, but also the nonlinear potential exhibits different behaviors along the x, y directions. We define the *anisotropy dimming* D_A as a quantity that is equal to one when the nonlinear potential is completely symmetric and is negative when ZS arises:

$$
D_A = \frac{\partial_y^2\Delta|_{\mathbf{r}_\perp=\mathbf{0}}}{\partial_x^2\Delta|_{\mathbf{r}_\perp=\mathbf{0}}}. \qquad (6)
$$

The anisotropy dimming corresponding to the initial condition $\psi_{\rm ANI}$ is $D_A = -2\sigma/\sqrt{\pi}$. Since $L_{\rm nloc} \propto \sqrt{|n_2|}$ [35], one obtains $D_A \propto -\sqrt{|n_2|}$.

Simulations corresponding to the asymmetric initial condition are illustrated in Fig. 2. Figure 2(a) shows the anisotropic DSWs, the solution of the NLSE, Eq. (1), with

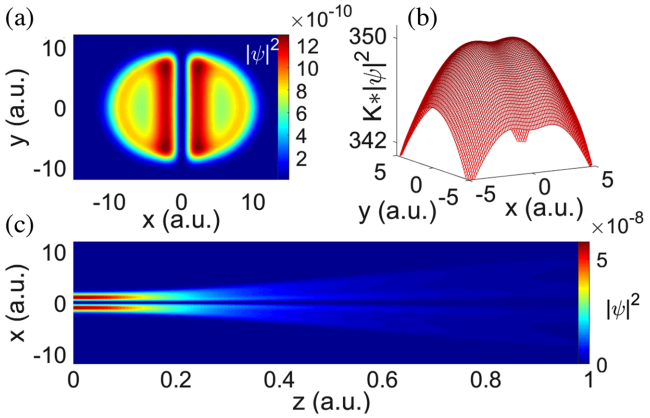

FIG. 2. Solution of the NLSE, Eq. (1), with an asymmetric initial condition, Eq. (5), for $P = 4 \times 10^6$ and $\sigma = 120$ in arbitrary units: (a) shows the intensity transverse profile at $z = 1$; (b) exhibits the asymmetric nonlinear potential; (c) reports the intensity longitudinal outline on the plane (x, z) with the zero singularity.

the initial condition Eq. (5). Figure 2(b) gives numerical proof of the nonlinear potential anisotropy: the (x, y)-plane origin corresponds to a saddle point with a locally increasing profile along $x > 0$, $y < 0$ and a locally decreasing outline along $x < 0$, $y > 0$. Figure 2(c) shows the side-view intensity pattern with ZS in a neighborhood of $x = 0$ during propagation.

The presence of the saddle point in the nonlinear potential in Fig. 2 changes the final model when, through highly nonlocal approximation, we map the NLSE into the quantumlike linear Schrödinger equation. From the expression of $\Delta(\mathbf{r}_\perp)$ above, for $\phi(\mathbf{r}) = e^{iP\Delta_0^2}\psi(\mathbf{r})$ we obtain

$$\begin{aligned} i\frac{\mathrm{d}}{\mathrm{d}z}|\phi(z)\rangle &= \hat{H}_{\mathrm{ANI}}(\mathbf{p}_\perp, \mathbf{r}_\perp)|\phi(z)\rangle, \\ \hat{H}_{\mathrm{ANI}}(\mathbf{p}_\perp, \mathbf{r}_\perp) &= \hat{H}_{\mathrm{HO}}(p_x, x)\mathbb{1}_y + \mathbb{1}_x\hat{H}_{\mathrm{RHO}}(p_y, y), \\ |\phi(z)\rangle &= |\phi_{\mathrm{odd}}(z)\rangle_x|\phi_{\mathrm{even}}(z)\rangle_y, \end{aligned} \tag{7}$$

where $\hat{H}_{\mathrm{HO}}(p_x,x)=\frac{1}{2}\hat{p_x}^2+(\omega^2/2)\hat{x}^2$ is the one-dimensional harmonic oscillator (HO) Hamiltonian with $\omega = \sqrt{P}\Delta_1$. The solution of Eq. (7) is the tensorial product of $|\phi_{\mathrm{odd}}(z)\rangle_x = \sum_{n=0}^{+\infty} e^{i(\omega/2)(2n+1)z}|\Psi_n^{\mathrm{HO}}\rangle\langle\Psi_n^{\mathrm{HO}}|\psi_{\mathrm{odd}}\rangle$, where $|\Psi_n^{\mathrm{HO}}\rangle$ are $\hat{H}_{\mathrm{HO}}$ eigenstates corresponding to the energy levels $E_n^{\mathrm{HO}} = (\omega/2)(2n+1)$ [55], and $|\phi_{\mathrm{even}}(z)\rangle_y = |\phi_N^G(z)\rangle + |\phi_N^{\mathrm{BG}}(z)\rangle$.

Evidence of the presence of GVs is given in Fig. 3. By defining

$$\Gamma_n = \gamma(2n+1), \tag{8}$$

we look for the first two quantized decay rates $\Gamma_{0,2}$ (the even Gaussian initial function only leads to even energy levels) in the longitudinal propagation in y direction. Indeed, if one computes the intensity of the y part, one finds $\langle\phi_{\mathrm{even}}(z)|\phi_{\mathrm{even}}(z)\rangle_y \overset{N\gg 0}{\simeq} \langle\phi_N^G(z)|\phi_N^G(z)\rangle = \sum_{n=0}^{N} e^{-\Gamma_n z}|\langle\mathfrak{f}_n^+|\phi_{\mathrm{even}}\rangle|^2$. Figure 3(a) shows numerical simulations of the nonlinear evolution. We seek decaying states by fixing $x = 2.29$ a little distant from the shock gap and report the corresponding intensity in the y–z plane. The pink line is equivalent to $x = y = 2.29$. Figure 3(b) exhibits $|\phi(x = 2.29, y = 2.29, z)|^2$, exponentially decaying. Two exponential fits demonstrate the GV occurrence: the fundamental Gamow state represents the plateau with decay rate $\Gamma_0 = 1.51$, whereas the first excited one interpolates the peak with decay rate $\Gamma_2 = 7.51$. We stress that the rule $\Gamma_2/\Gamma_0 = 5$ is respected, as generally defined in Eq. (8).

Our experiments are performed in isotropic thermal media (m-cresol/nylon solutions with 3.54% of nylon concentration [59], and hemoglobin solutions from lysed human red blood cells with a concentration of about 15 million cells per ml [33]), with both symmetric (in phase) and asymmetric (out of phase) initial conditions for the input beam. Experimental details can be found in the setup description in the Supplemental Material [70]. Figure 4 reports the experimental results obtained with the m-cresol/nylon thermal solution, where Fig. 4(a),(b) is from the input beam (enlargement of intensity and phase patterns at initial power $\bar{P} = 2$ mW and waist $W_0 = 25.9$ μm). The input beam presents a phase discontinuity of π along $x = 0$, as can be seen clearly from the magnified interferogram in Fig. 4(b). Under such an initial condition, wave breaking into asymmetric shock waves is observed at an appropriate level of nonlinearity, which

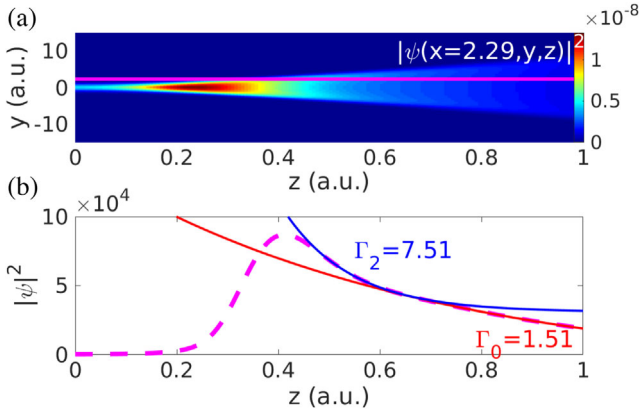

FIG. 3. GVs' signature. From Fig. 2, in the same conditions, (a) is the y, z profile at fixed $x = 2.29$. Intensity along the pink line, i.e., $|\phi(x{=}2.29,y{=}2.29,z)|^2{=}\langle\phi_{\mathrm{even}}(z)|\phi_{\mathrm{even}}(z)\rangle_y{=}\sum_{n=0}^{N}e^{-\Gamma_n z}|\langle\mathfrak{f}_n^+|\phi_{\mathrm{even}}\rangle|^2$, is plotted in (b) [Eq. (8) quantized decay rates]. The continuous lines represent the first two exponential functions of the summation above that fit the decaying part: the red line is the fundamental GV with decay rate Γ_0, and the blue line is the first excited GV with decay rate Γ_2.

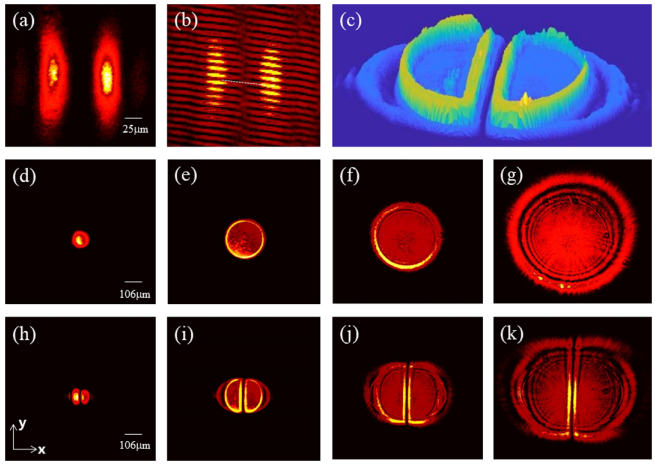

FIG. 4. Observation of wave dynamics in m-cresol/nylon thermal solution. (a) and (b) are the magnified intensity profile and phase pattern of the input beam under an out-of-phase condition. (c) is the 3D view of the splitting shock wave, where barriers and the gap are clearly visible. Middle and bottom rows are in-phase (d)–(g) and out-of-phase (h)–(k) output transverse intensity profiles at different initial powers (from left to right: 5 mW, 35 mW, 73 mW, and 112 mW).

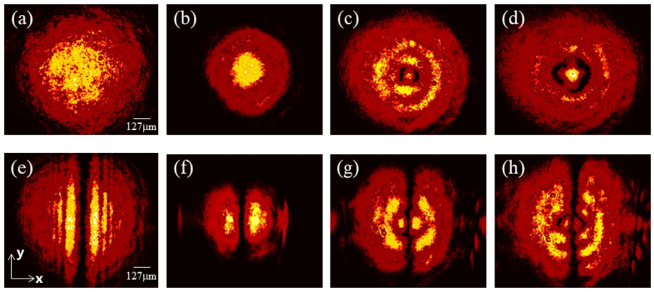

FIG. 5. Observation of wave dynamics in the hemoglobin solution. First (a)–(d) and second (e)–(h) rows show in-phase and out-of-phase output transverse intensity profiles, respectively, at different initial powers (from left to right: 5 mW, 150 mW, 233 mW, and 275 mW).

corresponds to our theoretical prediction in Fig. 2. A typical example is shown in Fig. 4(c), where the ZS can be seen clearly from the 3D plot. In the middle and bottom rows, we compare directly the beam dynamics observed for in-phase (middle row) and out-of-phase (bottom row) excitations under different levels of nonlinearity (as controlled by the input power). The output beam exhibits diffraction at a low power [Fig. 4(d), (h)] but evolves into an overall shock profile at high powers [Figs. 4(e)–4(g), 4(i)–4(k)]. The difference between the two excitation conditions is evident: the in-phase beam leads to a symmetric shock wave [Figs. 4(e)–4(g)], but the out-of-phase beam evolves into two parts with a clear barrier surrounding the gap [Figs. 4(i)–4(k)]. It is important to note that, while the whole profile expands, the gap between two parts remains nearly constant at a fixed power during propagation [the measured gap sizes for Figs. 4(h)–4(k) are (15.4 ± 1.6) μm, (12.3 ± 1.6) μm, (10.8 ± 1.6) μm, and (12.3 ± 1.6) μm]. This represents the first realization of what we define as *anisotropic DSWs*: an annular collapse singularity with an initial ZS that generates two barriers of light intensity around a constant gap in the middle of the beam. Despite the medium isotropy, the oddity of the initial condition generates an anisotropic final transverse profile.

We point out that the formation of anisotropic DSWs with distinct barriers depends on the strength of the self-defocusing, as stressed by the D_A definition in Eq. (6). For comparison, we perform similar experiments with a different thermal solution of hemoglobin (from lysed red blood cells), which also exhibits strong optical nonlinearity [33]. The results are shown in Fig. 5. Clearly, although the out-of-phase excitation develops asymmetric wave breaking [Fig. 5(h)], there is no barrier around the gap, even when the power is increased to 275 mW.

Z-scan measurements [71] of n_2 for both media are reported in the Supplemental Material [70]. The measured Kerr coefficients are $n_2 = -3.9 \times 10^{-8}$ cm^2/W for hemoglobin and $n_2 = -1.440 \times 10^{-6}$ cm^2/W for m-cresol/nylon, indicating that the hemoglobin nonlinearity is nearly 2 orders of magnitude smaller. As such, the asymmetric shock barrier cannot be achieved in the hemoglobin solutions before thermal convection takes place. Moreover, the final anisotropy dimming D_A for hemoglobin is one order of magnitude larger than the one for m-cresol/nylon [Eq. (6)]. These facts quantitatively explain the experimental need for giant nonlinearities in order to appreciate the anisotropic DSWs.

We point out that a few factors could account for the absence of evident anisotropic shocks in the hemoglobin solution as opposed to that in the m-cresol/nylon thermal solution. Apart from a smaller negative nonlinear coefficient, which slows down the development of the anisotropic shock, the differences in nonlocal response [72] and thermal convection [67] also contribute to the different beam dynamics in Fig. 5. In addition, we emphasize again that the asymmetry observed here results solely from the input beam condition, not the medium response itself.

We have proven that the interplay of a trapping (harmonic oscillator) and an antitrapping (reversed harmonic oscillator) potential generates a novel kind of dispersive shock waves, with the simultaneous presence of annular singularities and a shock gap enclosed by intense light barriers. The use of a thermal medium with a giant Kerr coefficient such as the m-cresol/nylon solution allows us to access an extremely nonlinear, highly nonlocal regime and perform accurate experiments to examine the asymmetric DSW dynamics. We modeled the outcoming dynamics through an advanced theoretical description in rigged Hilbert spaces by means of time asymmetric quantum mechanics, proving its intrinsic irreversibility. Our results not only confirm previous studies on the theoretical framework of DSWs in a highly nonlocal approximation and the giant nonlinear response of m-cresol/nylon but also disclose fundamental insights on the propagation of dispersive shock waves with a singular initial intensity profile in highly nonlinear nonlocal environments. We believe that this work can be a further step toward the description of complex annular collapse singularities where inverse scattering transform, Whitham modulation, and hydrodynamic approximation cannot provide descriptions as accurate as the ones given by time asymmetric quantum mechanics.

We are pleased to acknowledge support from the QuantERA ERA-NET Co-fund 731473 (Project QUOMPLEX), H2020 project Grant No. 820392, Sapienza Ateneo, PRIN 2015 NEMO, PRIN 2017 PELM, Joint Bilateral Scientific Cooperation CNR-Italy/RFBR-Russia, and the NSF Grant No. DMR-1308084.

*Corresponding author.
gmarcucc@uottawa.ca
†Corresponding author.
zhigang@sfsu.edu
‡Present address: Department of Physics, University of Ottawa, Ottawa, Ontario K1N 6N5, Canada.

[1] D. H. Peregrine, J. Fluid Mech. **25**, 321 (1966).
[2] N. F. Smyth and P. E. Holloway, J. Phys. Oceanogr. **18**, 947 (1988).
[3] M. D. Maiden, N. K. Lowman, D. V. Anderson, M. E. Schubert, and M. A. Hoefer, Phys. Rev. Lett. **116**, 174501 (2016).
[4] R. J. Taylor, D. R. Baker, and H. Ikezi, Phys. Rev. Lett. **24**, 206 (1970).
[5] B. Damski, Phys. Rev. A **69**, 043610 (2004).
[6] A. M. Kamchatnov, A. Gammal, and R. A. Kraenkel, Phys. Rev. A **69**, 063605 (2004).
[7] V. M. Pérez-García, V. V. Konotop, and V. A. Brazhnyi, Phys. Rev. Lett. **92**, 220403 (2004).
[8] T. P. Simula, P. Engels, I. Coddington, V. Schweikhard, E. A. Cornell, and R. J. Ballagh, Phys. Rev. Lett. **94**, 080404 (2005).
[9] M. A. Hoefer, M. J. Ablowitz, I. Coddington, E. A. Cornell, P. Engels, and V. Schweikhard, Phys. Rev. A **74**, 023623 (2006).
[10] J. J. Chang, P. Engels, and M. A. Hoefer, Phys. Rev. Lett. **101**, 170404 (2008).
[11] L. Romagnani, S. V. Bulanov, M. Borghesi, P. Audebert, J. C. Gauthier, K. Löwenbrück, A. J. Mackinnon, P. Patel, G. Pretzler, T. Toncian, and O. Willi, Phys. Rev. Lett. **101**, 025004 (2008).
[12] E. Bettelheim, A. G. Abanov, and P. Wiegmann, Phys. Rev. Lett. **97**, 246401 (2006).
[13] S. A. Akhmanov, D. P. Krindach, A. P. Sukhorukov, and R. V. Khokhlov, Sov. J. Exp. Theor. Phys. Lett. **6**, 38 (1967).
[14] J. E. Rothenberg and D. Grischkowsky, Phys. Rev. Lett. **62**, 531 (1989).
[15] G. A. El, A. Gammal, E. G. Khamis, R. A. Kraenkel, and A. M. Kamchatnov, Phys. Rev. A **76**, 053813 (2007).
[16] M. A. Hoefer and M. J. Ablowitz, Physica (Amsterdam) **236D**, 44 (2007).
[17] N. Ghofraniha, C. Conti, G. Ruocco, and S. Trillo, Phys. Rev. Lett. **99**, 043903 (2007).
[18] W. Wan, S. Jia, and J. W. Fleischer, Nat. Phys. **3**, 46 (2007).
[19] C. Conti, A. Fratalocchi, M. Peccianti, G. Ruocco, and S. Trillo, Phys. Rev. Lett. **102**, 083902 (2009).
[20] N. Ghofraniha, S. Gentilini, V. Folli, E. DelRe, and C. Conti, Phys. Rev. Lett. **109**, 243902 (2012).
[21] J. Garnier, G. Xu, S. Trillo, and A. Picozzi, Phys. Rev. Lett. **111**, 113902 (2013).
[22] S. Gentilini, N. Ghofraniha, E. DelRe, and C. Conti, Phys. Rev. A **87**, 053811 (2013).
[23] S. Gentilini, F. Ghajeri, N. Ghofraniha, A. D. Falco, and C. Conti, Opt. Express **22**, 1667 (2014).
[24] V. Smith, P. Cala, W. Man, and Z. Chen, in *CLEO: 2014* (Optical Society of America, Washington, DC, 2014), p. FW3D.1.
[25] S. Gentilini, M. C. Braidotti, G. Marcucci, E. DelRe, and C. Conti, Phys. Rev. A **92**, 023801 (2015).
[26] S. Gentilini, M. C. Braidotti, G. Marcucci, E. DelRe, and C. Conti, Sci. Rep. **5**, 15816 (2015).
[27] G. Xu, D. Vocke, D. Faccio, J. Garnier, T. Roger, S. Trillo, and A. Picozzi, Nat. Commun. **6**, 8131 (2015).
[28] M. C. Braidotti, S. Gentilini, and C. Conti, Opt. Express **24**, 21963 (2016).
[29] B. Wetzel, D. Bongiovanni, M. Kues, Y. Hu, Z. Chen, S. Trillo, J. M. Dudley, S. Wabnitz, and R. Morandotti, Phys. Rev. Lett. **117**, 073902 (2016).
[30] G. Xu, A. Mussot, A. Kudlinski, S. Trillo, F. Copie, and M. Conforti, Opt. Lett. **41**, 2656 (2016).
[31] G. Xu, J. Garnier, D. Faccio, S. Trillo, and A. Picozzi, Physica (Amsterdam) **333D**, 310 (2016).
[32] A. Zannotti, M. Rüschenbaum, and C. Denz, J. Opt. **19**, 094001 (2017).
[33] R. Gautam, Y. Xiang, J. Lamstein, Y. Liang, A. Bezryadina, G. Liang, T. Hansson, B. Wetzel, D. Preece, A. White, M. Silverman, S. Kazarian, J. Xu, R. Morandotti, and Z. Chen, Light **8**, 31 (2019).
[34] G. Marcucci, D. Pierangeli, A. J. Agranat, R. K. Lee, E. DelRe, and C. Conti, Nat. Commun. **10**, 5090 (2019).
[35] G. Marcucci, D. Pierangeli, S. Gentilini, N. Ghofraniha, Z. Chen, and C. Conti, Adv. Phys. X **4**, 1662733 (2019).
[36] R. W. Boyd, *Nonlinear Optics*, 3rd ed. (Academic Press, New York, 2008).
[37] G. Xu, A. Fusaro, J. Garnier, and A. Picozzi, Appl. Sci. **8**, 2559 (2018).
[38] C. S. Gardner, J. M. Greene, M. D. Kruskal, and R. M. Miura, Phys. Rev. Lett. **19**, 1095 (1967).
[39] V. E. Zacharov and A. B. Shabat, Sov. Phys. JEPT **34**, 62 (1972).
[40] G. Fibich, *The Nonlinear Schrödinger Equation* (Springer International Publishing, New York, 2015).
[41] T. P. Horikis and D. J. Frantzeskakis, Phys. Rev. Lett. **118**, 243903 (2017).
[42] T. P. Horikis and D. J. Frantzeskakis, Proc. R. Soc. A **475**, 20190110 (2019).
[43] G. B. Whitham, *Linear and Nonlinear Waves* (Wiley, New York, 1999).
[44] A. Bohm, J. Math. Phys. (N.Y.) **22**, 2813 (1981).
[45] A. Bohm, M. Gadella, and G. B. Mainland, Am. J. Phys. **57**, 1103 (1989).
[46] A. Bohm and N. L. Harshman, Lect. Notes Phys. **504**, 179 (1998).
[47] A. Bohm, Phys. Rev. A **60**, 861 (1999).
[48] D. Chruściński, Open Syst. Inf. Dyn. **09**, 207 (2002).
[49] R. de la Madrid and M. Gadella, Am. J. Phys. **70**, 626 (2002).
[50] M. Gadella and F. Gomez, Int. J. Theor. Phys. **42**, 2225 (2003).
[51] D. Chruściński, J. Math. Phys. (N.Y.) **44**, 3718 (2003).
[52] D. Chruściński, J. Math. Phys. (N.Y.) **45**, 841 (2004).
[53] O. Civitarese and M. Gadella, Phys. Rep. **396**, 41 (2004).
[54] E. Celeghini, M. Gadella, and M. A. del Olmo, J. Math. Phys. (N.Y.) **57**, 072105 (2016).
[55] G. Marcucci and C. Conti, Phys. Rev. A **94**, 052136 (2016).
[56] G. Marcucci, M. C. Braidotti, S. Gentilini, and C. Conti, Ann. Phys. (Berlin) **529**, 1600349 (2017).
[57] G. Gamow, Z. Phys. **51**, 204 (1928).
[58] G. Gamow, Nature (London) **122**, 805 (1928).
[59] V. Smith, B. Leung, P. Cala, Z. Chen, and W. Man, Opt. Mater. Express **4**, 1807 (2014).
[60] A. Einstein, Ann. Phys. (Berlin) **322**, 549 (1905).
[61] S. Fardad, A. Salandrino, M. Heinrich, P. Zhang, Z. Chen, and D. N. Christodoulides, Nano Lett. **14**, 2498 (2014).
[62] A. L. Marchant, T. P. Billam, T. P. Wiles, M. M. Yu, S. A. Gardiner, and S. L. Cornish, Nat. Commun. **4**, 1865 (2013).
[63] V. Tikhonenko, J. Christou, B. Luther-Davies, and Y. S. Kivshar, Opt. Lett. **21**, 1129 (1996).

[64] M. Lisak, B. A. Malomed, and D. Anderson, Opt. Lett. **16**, 1936 (1991).
[65] A. W. Snyder and D. J. Mitchell, Science **276**, 1538 (1997).
[66] C. Conti, M. Peccianti, and G. Assanto, Phys. Rev. Lett. **91**, 073901 (2003).
[67] A. Minovich, D. N. Neshev, A. Dreischuh, W. Krolikowski, and Y. S. Kivshar, Opt. Lett. **32**, 1599 (2007).
[68] S. Ouyang, Q. Guo, and W. Hu, Phys. Rev. E **74**, 036622 (2006).
[69] V. Folli and C. Conti, Opt. Lett. **37**, 332 (2012).
[70] See Supplemental Material at http://link.aps.org/supplemental/10.1103/PhysRevLett.125.243902 for theoretical further analysis, experimental setup, Z-scan measurements, and shock-gap behavior.
[71] M. Sheik-bahae, A. A. Said, and E. W. V. Stryland, Opt. Lett. **14**, 955 (1989).
[72] K. Cyprych, P. S. Jung, Y. Izdebskaya, V. Shvedov, D. N. Christodoulides, and W. Krolikowski, Opt. Lett. **44**, 267 (2019).